Naval Research Laboratory
Washington, DC 20375-5320

NRL/MR/6324--98-8185

Continuous Cooling Transformation (CCT) Diagrams for Advanced Navy Welding Consumables

R. W. FONDA
R. A. VANDERMEER
G. SPANOS

Physical Metallurgy Branch
Materials Science and Technology Division

July 15, 1998

REPORT DOCUMENTATION PAGE

Form Approved
OMB No. 0704-0188

1. AGENCY USE ONLY (*Leave Blank*)	2. REPORT DATE	3. REPORT TYPE AND DATES COVERED
	July 15, 1998	Progress Report, March 1997-March 1998

4. TITLE AND SUBTITLE

Continuous Cooling Transformation (CCT) Diagrams for Advanced Navy Welding Consumables

5. FUNDING NUMBERS

63-5795-0-7

6. AUTHOR(S)

R.W. Fonda, R.A. Vandermeer, and G. Spanos

7. PERFORMING ORGANIZATION NAME(S) AND ADDRESS(ES)

Naval Research Laboratory
Washington, DC 20375-5320

8. PERFORMING ORGANIZATION REPORT NUMBER

NRL/MR/6324--98-8185

9. SPONSORING/MONITORING AGENCY NAME(S) AND ADDRESS(ES)

Office of Naval Research
800 N. Quincy Street
Arlington, VA 22217

10. SPONSORING/MONITORING AGENCY REPORT NUMBER

11. SUPPLEMENTARY NOTES

12a. DISTRIBUTION/AVAILABILITY STATEMENT

Approved for public release; distribution is unlimited.

12b. DISTRIBUTION CODE

13. ABSTRACT (*Maximum 200 words*)

We have characterized the transformation behavior and microstructural evolution of new ultra-low carbon (ULC) welding consumables being developed for Naval applications by the National Center for Excellence in Metalworking Technology (NCEMT). This is the first systematic study of these ULC alloys combining dilatometric analysis and transmission electron microscopy (TEM) with more conventional characterization techniques to identify in detail the microstructures produced at various cooling rates and develop continuous cooling transformation (CCT) diagrams for these new weld consumables. CCT diagrams of these NCEMT ULC alloys have been developed for (I) *as-deposited* weld metal from a weldment of HSLA-100 base plate welded with the "CTC-08" weld consumable and (II) weld rods representing the extreme rich and lean compositional variants expected for production quantities of the "CTC-03" weld consumable. These results are compared to each other, to the results of our earlier examination of the HSLA-100 base metal, and to the literature on some low carbon alloys. One of the important findings of this study is that the compositional variations expected from production heats cause extensive variations in the transformation behavior, microstructure, and microhardness of these ULC consumables. Since current fabrication practices would generate a similar compositional variation for any comparable ULC alloy, additional steps need to be taken to ensure the chemical homogeneity, and thus uniform weld properties, of the ULC weld consumables.

14. SUBJECT TERMS

CCT Diagram
Ultra-low Carbon (ULC) Steels
Welding
Microstructure

15. NUMBER OF PAGES

31

16. PRICE CODE

17. SECURITY CLASSIFICATION OF REPORT	18. SECURITY CLASSIFICATION OF THIS PAGE	19. SECURITY CLASSIFICATION OF ABSTRACT	20. LIMITATION OF ABSTRACT
UNCLASSIFIED	UNCLASSIFIED	UNCLASSIFIED	UL

NSN 7540-01-280-5500

Standard Form 298 (Rev. 2-89)
Prescribed by ANSI Std 239-18
298-102

CONTENTS

CONTINUOUS COOLING TRANSFORMATION (CCT) DIAGRAMS FOR ADVANCED NAVY WELDING CONSUMABLES

INTRODUCTION

High yield strength (HY) steels, which have been used extensively in Naval ship construction, are being replaced in many applications by high-strength low-alloy (HSLA) steels [1,2]. While HSLA steels can be processed to have an excellent combination of strength and toughness, it is the potential to significantly reduce fabrication costs through the reduction or elimination of preheat, relaxation of stringent interpass temperature controls, and expansion of the usable heat input range which has driven this replacement [2,3]. Despite this, adequate weld filler metals for realizing these cost reduction measures while welding these HSLA steels are not yet available, so weld consumables developed for the HY steels are currently being used to weld the newer HSLA steels [2]. Thus, there is a current need to develop new ULC weld consumables for welding these modern HSLA steels with reduced preheat and reduced controls on the interpass temperature and heat input. This requires an understanding of the phase transformation behavior of these ULC alloys and how those phase transformations are affected by changes in the weld consumable chemistry and cooling rate.

An additional complication with these new ULC weld consumables is the compositional accuracy of current processes for the fabrication of production quantities of these steels. For the low alloy content of these steels (particularly carbon), the standard chemical variations for a production heat can be significant. It is critical to understand the potential impact of these production variations on the microstructures and properties of these ULC steels. This is the topic of the second portion of this report, in which we investigated the variations in transformation behavior, microstructure, and microhardness for the potential extreme compositions (rich and lean) which could result from compositional variations from the vendor.

The phase transformation behavior of a material can be displayed as a function of cooling rate on a continuous cooling transformation (CCT) diagram [4]. CCT diagrams can be used to predict the microstructures, and thus the properties, which would result from a specific cooling rate, whether due to fabrication, thermal processing, or welding, and as such are important for engineers and designers in the development, processing and use of new materials. In welding processes, these CCT diagrams can be used to help define the welding operational envelope for fabrication of a weldment which satisfies the necessary specifications. Similarly, CCT diagrams serve as a quick reference on cooling rates to avoid in order to prevent the formation of deleterious microstructures, which could be too hard, too soft, susceptible to hydrogen-assisted cracking, etc. The CCT diagrams developed for these NCEMT consumables are critical, since very little standardized information of this type is available for any of these advanced ULC consumables. This study thus provides a quantitative baseline for understanding and controlling

microstructural evolution in ULC consumables. This report is divided into two parts: (I) a study of *as-deposited* weld metal from a weldment of HSLA-100 base plate welded with the ULC weld consumable "CTC-08", and (II) an investigation of weld rods representing the extreme rich and lean compositional variants expected for production quantities of the "CTC-03" ULC weld consumable.

I. DILATOMETRIC AND MICROSTRUCTURAL ANALYSIS OF *AS-DEPOSITED* CTC-08 WELD METAL

The primary effort of this part of the project was on the development of a CCT diagram for *as-deposited* weld metal and correlation of the microstructures to those observed in actual weldments. Dilatometric samples removed from as-deposited weldments were thermally cycled at a variety of cooling rates then characterized by optical microscopy, transmission electron microscopy, microhardness measurements, and prior austenite grain size measurements to determine the microstructures produced under various cooling rates. Criteria were also developed to differentiate between the two predominant microstructures in these steels, lath martensite and lath ferrite, which can look quite similar but which have very different properties. Comparisons between these microstructures and those observed in actual weldments of the same composition are in progress and will be described in a later report.

Experimental Procedure

The dilatometric samples were removed from the center of a multipass Gas Metal Arc (GMA) weldment prepared with the CTC-08 filler metal (a MIL-120S candidate filler metal developed by NCEMT) and 1" thick HSLA-100 base plate. Although the composition of this low carbon, Mn-Ni-Mo-Ti consumable is proprietary, the carbon level of the as-deposited weld metal (0.04%) will be referred to throughout this report. The cylindrical 3 mm diameter by approximately 10 mm long samples were cored directly out of the weldment by electro-discharge machining with a hollow cylindrical electrode. The weldment from which these samples were cored (CTC-08A) was prepared at a heat input of 55 kJ/in heat input. This low heat input weldment was selected to minimize potential chemical variations between the different dilatometry samples. Samples were only removed from three weld beads at the top center of this 16-bead weldment. These three weld beads were not adjacent to the base plate and were more than three beads removed from the root passes, minimizing potential variations due to dilution. Significant variations in the transformation behavior were observed in samples obtained from outside these three beads. *

These samples were thermally cycled with a heating/quenching dilatometer. They were heated to 1200 °C, where they were held for 15 minutes, then cooled at various rates with Newtonian cooling such that the cooling rate is proportional to the temperature difference between the sample and its surroundings. Fifteen different cooling rates were employed, with $t_{8/5}$'s (the time to cool from 800 °C to 500 °C) ranging from 1.1 s to 3016 s. (A smaller $t_{8/5}$ corresponds to a faster cooling rate, and vice-versa).

---

* Effects of compositional variations on microstructure and properties across weldments are currently being addressed in a separate project in our group at the Naval Research Laboratory.

Results and Discussion

Transformation Curves and "Unlabeled " CCT diagram

The slight expansions or contractions which accompany phase transitions are readily observed by dilatometry. Thus, the volume fraction of austenite (the high temperature phase) transformed as a function of temperature can readily be calculated after subtracting out the relative contributions due to the coefficients of thermal expansion of the parent (austenite) and product phases [4]. One of the primary uses of transformation curves such as that shown in Figure 1, is to determine the start temperature of austenite decomposition for a particular cooling rate. It is evident that these as-deposited weld metal samples can be grouped according to three distinct transformation start temperatures. At the fastest cooling rates ($t_{8/5}$ = 1.1 s to $t_{8/5}$ = 2.2 s), the weld metal starts transforming at about 400 °C. This represents the martensite start temperature, M_s, as verified by microstructural analysis (see the Microstructural Analysis sub-section below). For a wide range of intermediate cooling rates (from $t_{8/5}$ = 3.8 s to $t_{8/5}$ = 301 s), encompassing most cooling rates typically used in GMA welding, the austenite begins to transform at about 460 °C to 480 °C. This will be shown to correspond to the initial formation of lath ferrite. The slowest cooling rates ($t_{8/5} \geq 516$ s) exhibit an additional transformation start temperature at 530 °C.

The cooling curves (Fig. 2) reveal that samples cooled at intermediate cooling rates, particularly $t_{8/5}$ = 28 s, 52 s, and 100 s, experience a significant recalescence (reheating of the sample) during decomposition from the high-temperature austenite phase. While recalescence was also observed during our dilatometric examination of the CTC-03 weld wire compositions (see below), no recalescence was observed in our examination of the HSLA-100 base plate.

The transformation start (1% transformation) and transformation finish (99.5% transformation) times and temperatures for each cooling rate are readily determined from the transformation curves (Fig. 1). These times and temperatures are used to construct an "unlabeled" CCT diagram by plotting the transformation start and finish points for each cooling rate on a graph in which the y-axis is temperature and the x-axis is time. This diagram will subsequently be labeled according to the microstructural observations (see the Microstructural Analysis section and Fig. 11 below).

Prior Austenite Grain Size

Because it can strongly affect the decomposition of the high-temperature austenite phase to low-temperature constituents such as ferrite or martensite (see e.g., [5]), the prior austenite grain size was measured for the fast, moderate, and slow cooling rates ($t_{8/5}$ = 2.2 s, 301 s, and 3016 s) to determine the effect of cooling rate on the austenite grain size. These measurements revealed an essentially constant prior austenite grain size of about 41 microns for the different cooling rates. There was no significant grain growth even during the slowest cooling cycles.

Microhardness

In addition to providing a measure of property variations resulting from different thermal cycles, microhardness can give an indication of the local microstructure, since the different phases that form can have significantly different hardness levels,. The variation in microhardness resulting from the different thermal cycles is shown in Figure 3. The microhardness is essentially constant at 335 H_v for all of the fastest cooling rates with $t_{8/5}$'s under 10 s. As will be shown

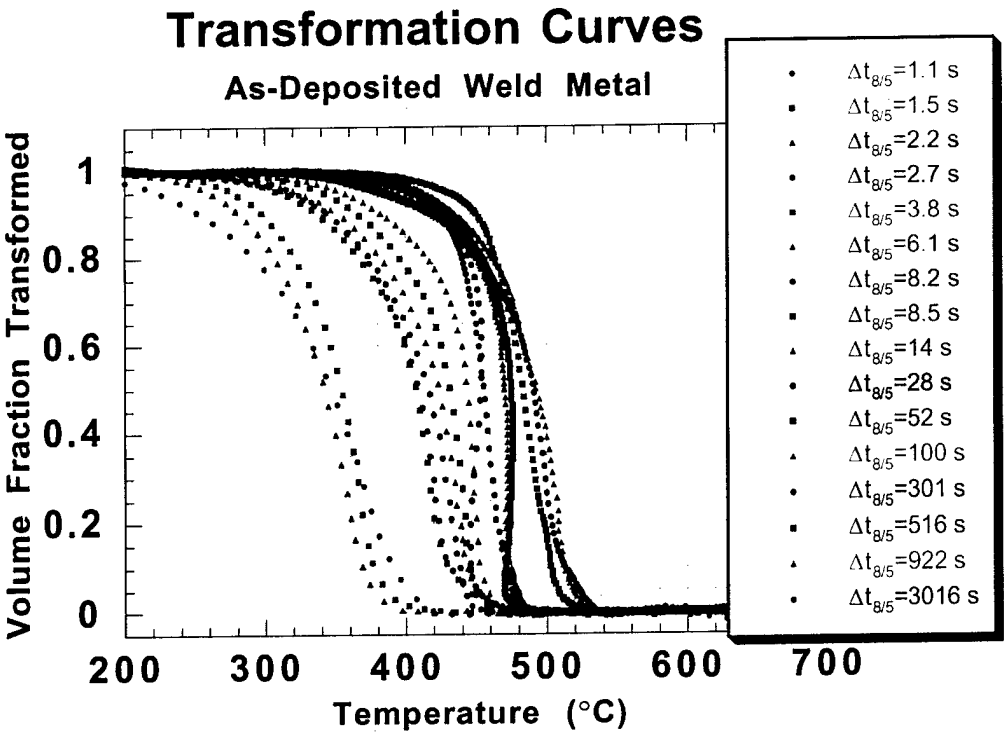

Figure 1. Transformation curves showing volume fraction of austenite transformed for different $t_{8/5}$'s (cooling times between 800 °C and 500 °C) in CTC-08 as -deposited weld metal.

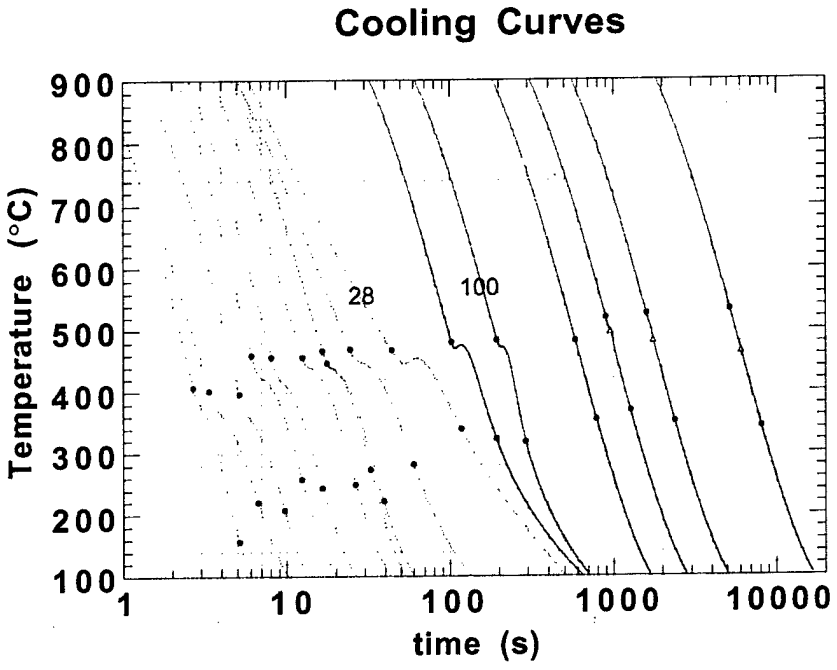

Figure 2. Cooling curves for different $t_{8/5}$'s ($t_{8/5}$'s of 28 and 100 are labeled) for dilatometry specimens taken from the CTC-08 as -deposited weld metal.

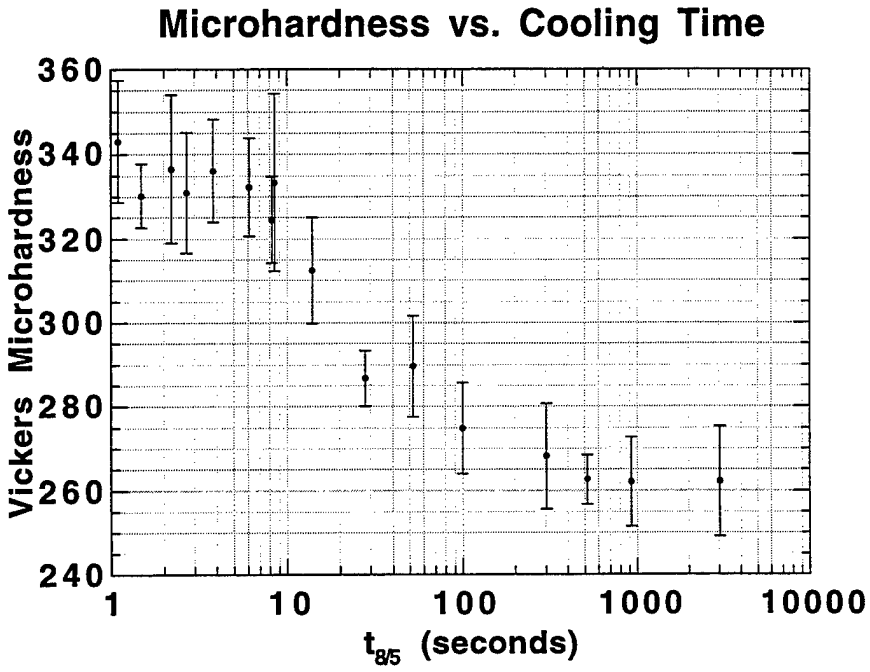

Fig. 3: Microhardness as a function of $t_{8/5}$, the cooling time between 800 °C and 500 °C ($t_{8/5}$ is inversely proportional to cooling rate).

later, this microhardness is characteristic of a predominantly martensitic microstructure. Similarly, the slowest cooling rates, with $t_{8/5}$'s of 516 or more, have a constant microhardness of approximately 263 H_V. This microhardness will be shown to correspond to a microstructure consisting predominantly of degenerate lath ferrite. At intermediate cooling rates, from $t_{8/5}$ = 14 s to $t_{8/5}$ = 301 s, the microhardness gradually decreases with increasing cooling times, reflecting both a decrease in the amount of martensite and an increasing degeneracy of the ferrite in these microstructures (see below).

Microstructural Analysis - Optical Microscopy

Initial observations by optical microscopy of the microstructures produced at the various cooling rates (Fig. 4) reveal pronounced differences in the final microstructures as the cooling rate is decreased from a $t_{8/5}$ of 2.2 s to a $t_{8/5}$ of 3016 s. The fastest cooling rates (e.g., $t_{8/5}$ = 2.2 s) produce a microstructure which is not well resolved at the optical microscopy level of resolution, but is consistent with a predominantly lath martensite morphology. The microstructures produced at intermediate cooling rates ($t_{8/5}$ = 28 s or 100 s) appear at this level of resolution to be predominantly conventional lath ferrite. The slowest cooling rate ($t_{8/5}$ = 3016 s) results in a microstructure characteristic of "ferrite with non-aligned second phase (FS(NA))" [6]. The microstructures produced at transitional cooling rates between those resulting in more conventional microstructures (e. g., $t_{8/5}$ = 8.5 s or 301 s) are not as readily identified, and it will be demonstrated later that even apparently conclusive optical microscopy results can be misleading due to the resolution limits of that technique. Particularly at the intermediate cooling rates (which includes a substantial range of the cooling rates typically used in GMA welding),

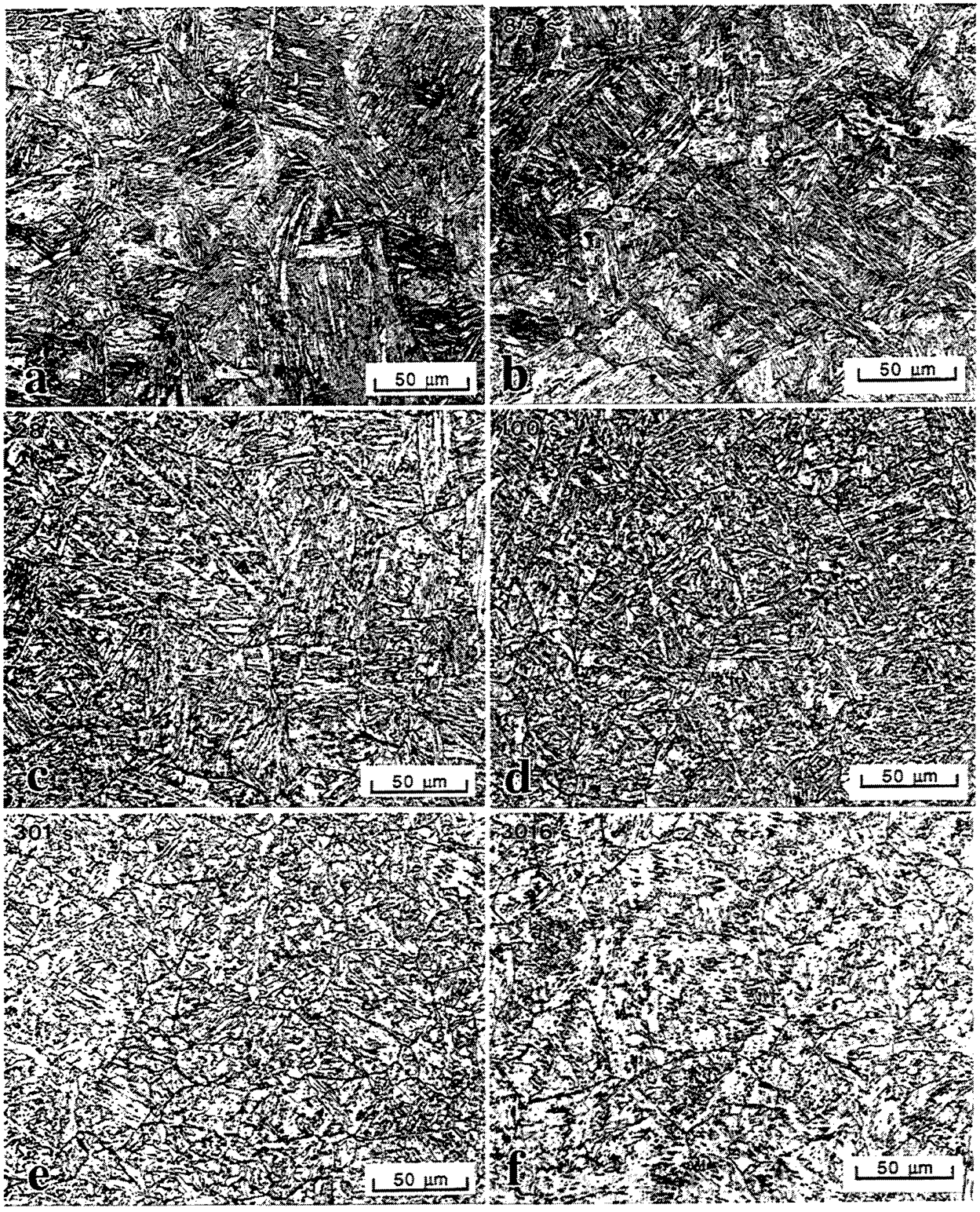

Figure 4. Optical micrographs of CTC-08 as-deposited weld metal subjected to dilatometry cycles with cooling rates corresponding to $t_{8/5}$ times of: (a) 2.2 s, (b) 8.5 s, (c) 28 s, (d) 100 s, (e) 301 s, and (f) 3016 s.

optical microscopy does not provide sufficient resolution to adequately identify the microconstituents in these alloys. To obtain the necessary resolution to distinguish between the microconstituents in these ULC alloys, transmission electron microscopy (TEM) must be employed.

Microstructural Analysis - Transmission Electron Microscopy

Transmission electron microscopy verifies that the microstructure produced by the three fastest cooling rates ($t_{8/5}$ = 1.1 s, 1.5 s, and 2.2 s) is fully martensitic (Figure 5). As shown in Fig. 5, the martensite consists of both fine lath martensite and a coarse martensite which was recently discovered and characterized in HSLA-100 steel at NRL [7]. The coarse martensite is more prevalent at faster cooling rates. TEM was used to further characterize this microstructure and to develop criteria for the differentiation between fine lath ferrite and fine lath martensite. Distinctive features of the fine lath martensite are: (1) different lath orientation variants within a packet, often leading to (2) significant crystallographic misorientations (high-angle boundaries) between adjacent laths, (3) linear/straight interlath boundaries, and (4) long thin planar sheets of retained austenite at interlath boundaries (appear as dark lines in bright field TEM images).

For the faster cooling rates generally applicable to welding ($t_{8/5}$ = 2.7 s to 8.5 s), it is quite difficult to determine the microstructure by optical microscopy (Figure 4). TEM of these samples reveals a predominantly lath martensitic microstructure containing a small amount of a coarse plate martensite, and some long laths of ferrite - Fig. 6. This is consistent both with the transformation temperatures (above M_S) observed by dilatometry and with the high microhardness observed.

Microstructures produced by moderate cooling rates ($t_{8/5}$ = 14 s to 52 s), corresponding to typical welding conditions, appear to range from mostly to fully ferritic by optical microscopy (Figure 4(c)). However, TEM observations reveal these to be mixed microstructures ranging from predominantly martensitic ($t_{8/5}$ = 14 s) to predominantly ferritic ($t_{8/5}$ = 52 s), with pockets of interlath retained austenite. The reason for this discrepancy is that the ferrite initially forms as long, isolated laths which are readily observed by optical microscopy while the packets of ferrite and martensite which form later between these laths are not readily resolved by that technique but can readily be resolved by TEM - see Fig. 7. In contrast to the fine lath martensite, the distinctive features of lath ferrite apparent by TEM (see Figures 7 and 8) are: (1) few, and usually only one, lath variant(s) within each packet, causing laths to be often parallel, (2) similar crystallographic orientations of ferrite laths resulting in (3) low-angle interlath boundaries, (4) curved or wavy interlath boundaries, and (5) blocky or truncated regions of retained austenite. Further comparisons reveal that lath ferrite has (6) a coarser lath morphology and (7) a higher carbon content (readily measured by Parallel Electron Energy Loss Spectroscopy) than lath martensite. Through this range of cooling rates, the microhardness displays a marked decrease from predominantly martensitic (near 335 H_V) to predominantly ferritic (about 270 H_V), consistent with the above TEM observations.

At cooling times of $t_{8/5}$ = 100 s or more (slower cooling than most typical welding conditions) the microstructure appears fully ferritic by both optical microscopy (Figures 4(d) - (f)) and TEM (Figures 8 and 9). As the cooling time increases, the appearance of this ferrite becomes more degenerate (sometimes referred to as "ferrite with non-aligned second phase" [6]),

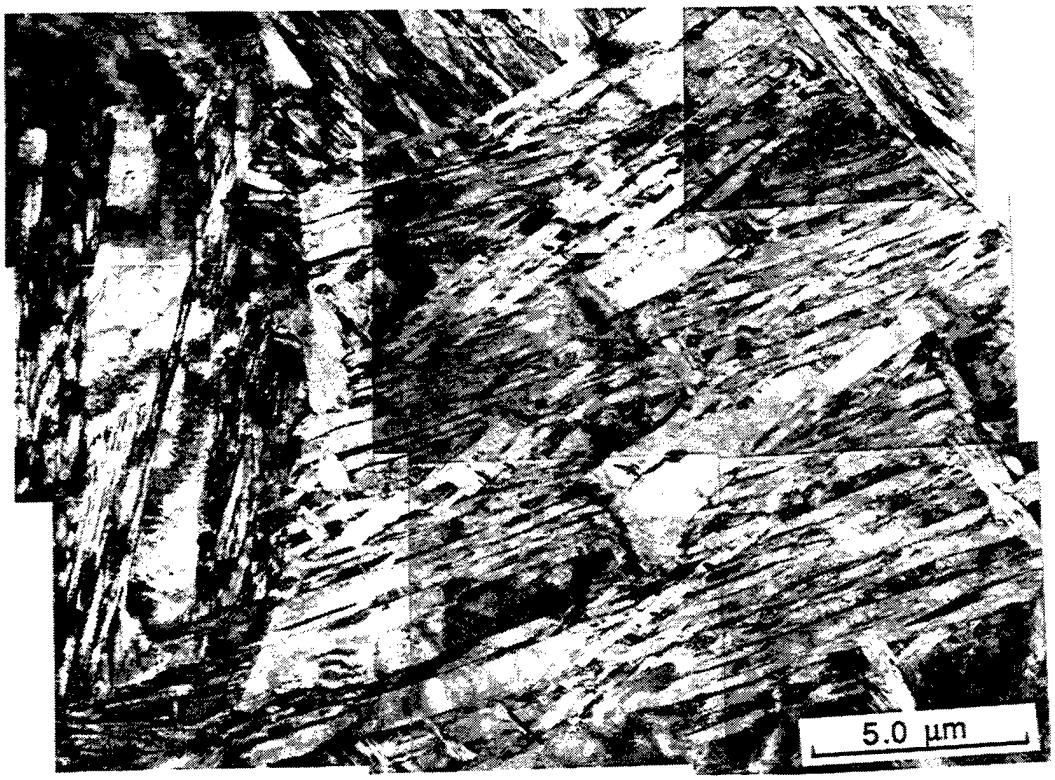

Figure 5. TEM micrograph of CTC-08 as-deposited weld metal specimen subjected to a cooling cycle with a $t_{8/5}$ of 2.2 s.

Figure 6. TEM micrograph of CTC-08 as-deposited weld metal ($t_{8/5}$ = 2.2 s) showing coarse martensite (CM), fine lath martensite (M), ferrite laths (F) and inclusions (I).

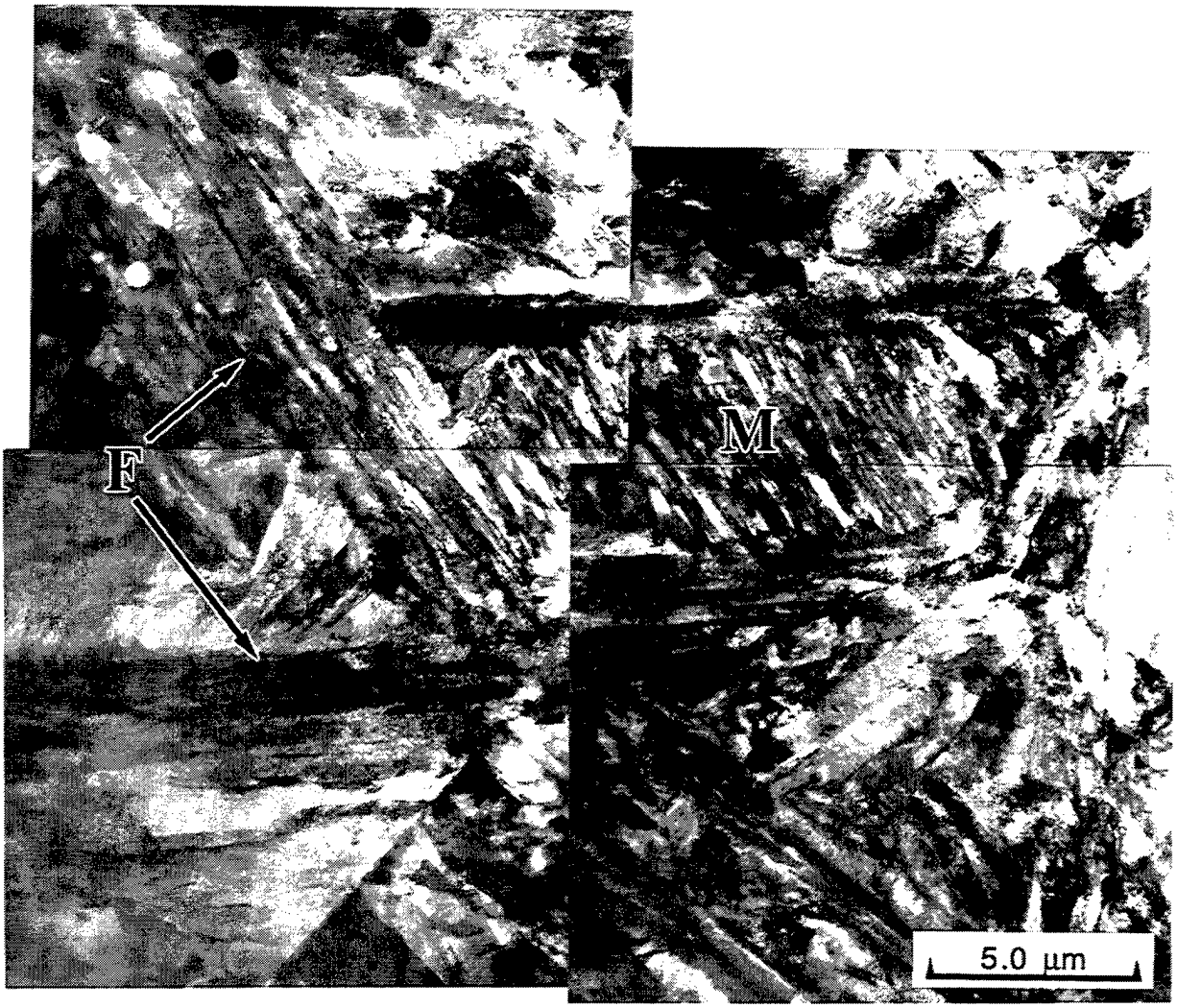

Fig. 7: TEM micrograph of CTC-08 weld metal subjected to a cooling cycle with a $t_{8/5}$ of 28 s, showing regions of lath martensite (M) and elongated lath ferrite (F).

i.e., the laths become less well-defined due to minimal or absent contrast between individual laths and the retained austenite becomes more blocky and angular - Fig. 10. This usually leads to a somewhat equiaxed appearance of the ferrite packets.

CCT Diagrams with Labeled Phase Fields

Based on the dilatometric, microstructural and microhardness observations, the CCT diagram for the as-deposited weld metal was labeled as shown in Fig. 11. The martensite start temperature, determined by the three fastest cooling rates (the three leftmost transformation start points on the diagram), is approximately 400 °C. Long ferrite laths start to form for cooling times of at least $t_{8/5}$ = 2.7 s (corresponding to the fourth transformation start point from the left in Fig. 11). As cooling rates decrease (i.e. for larger $t_{8/5}$s), packets of lath ferrite form around these large laths until, at $t_{8/5}$ = 28 s, lath ferrite becomes the majority phase. The ferrite starts developing a degenerate appearance at $t_{8/5}$ = 100 s. At slower cooling rates (beginning at approximately $t_{8/5}$ = 516 s - the third transformation start point from the right in Fig. 11), a

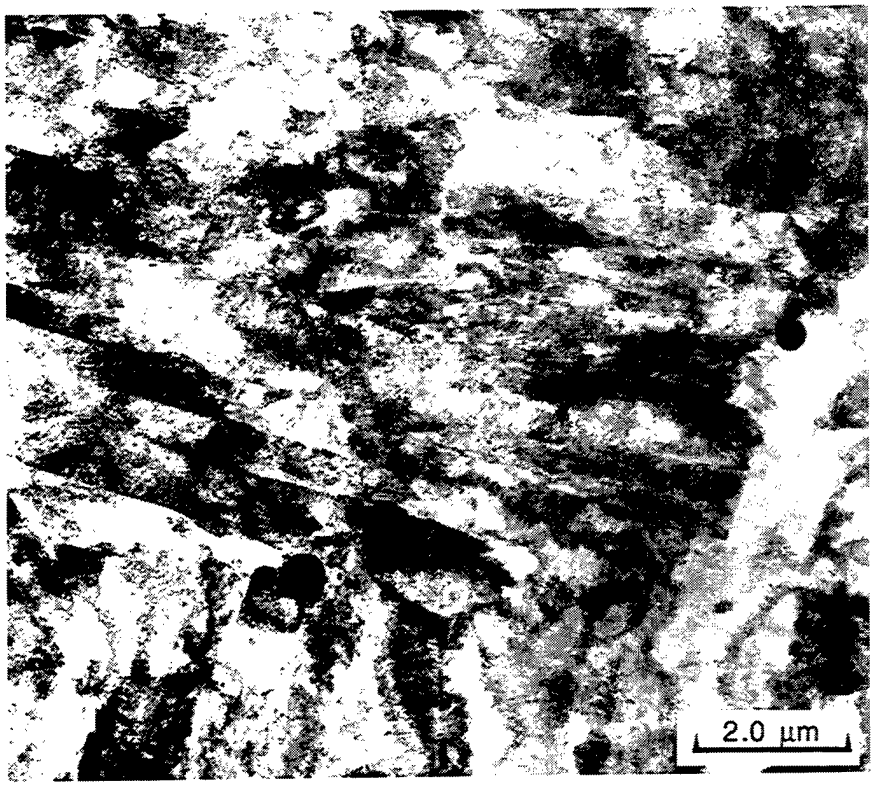

Figure 8. TEM micrograph of ferrite in CTC-08 weld metal subjected to a cooling cycle with a $t_{8/5}$ of 100 s.

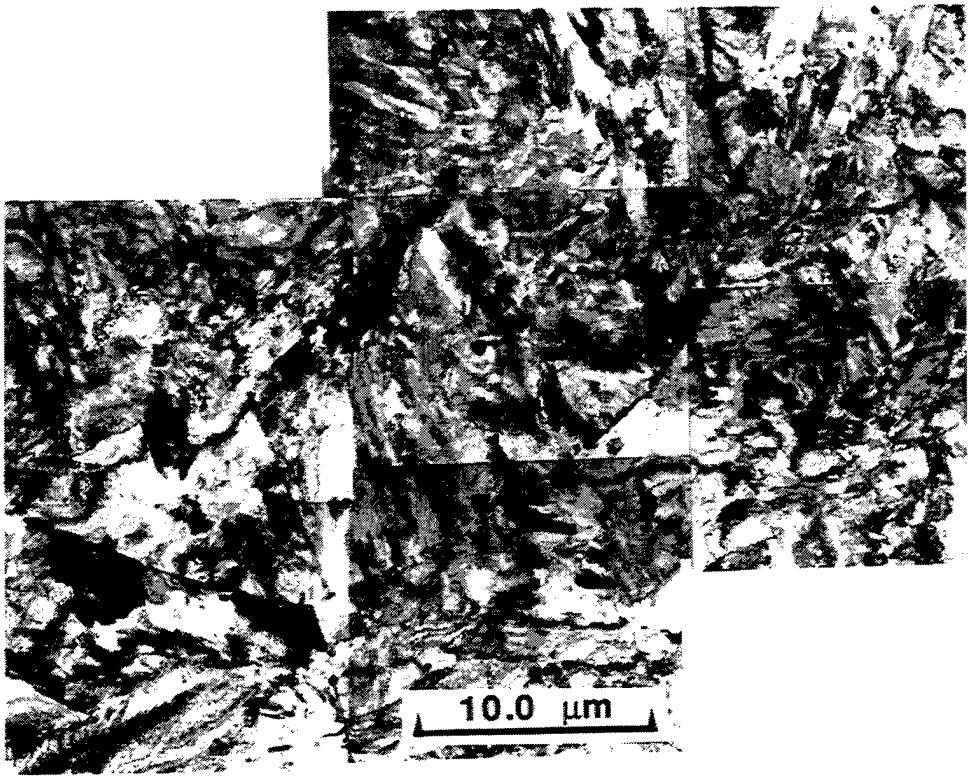

Figure 9. TEM micrograph of CTC-08 weld metal subjected to a cooling cycle with a $t_{8/5}$ of 301 s.

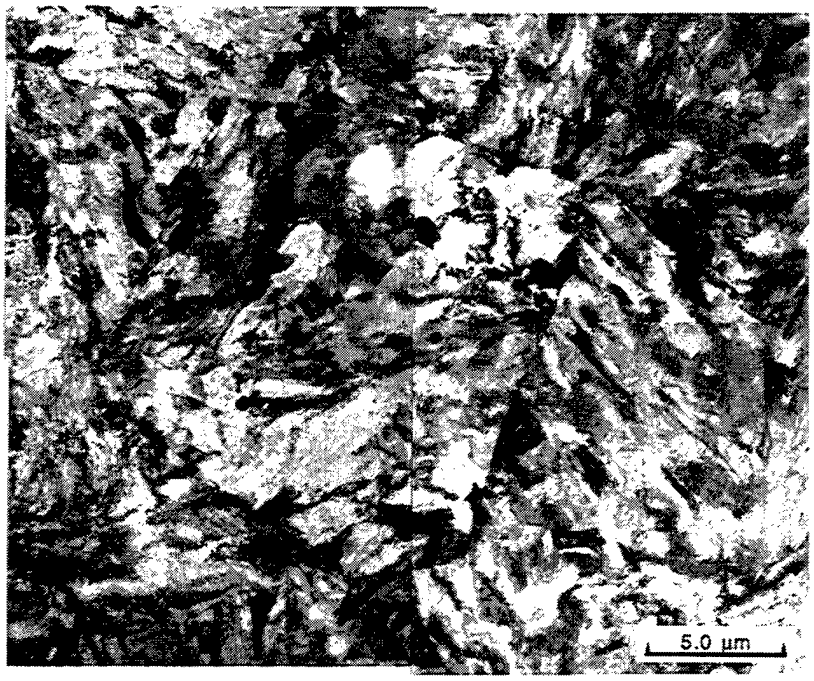

Figure 10. TEM micrograph of degenerate ferrite in CTC-08 weld metal ($t_{8/5}$ = 3016 s).

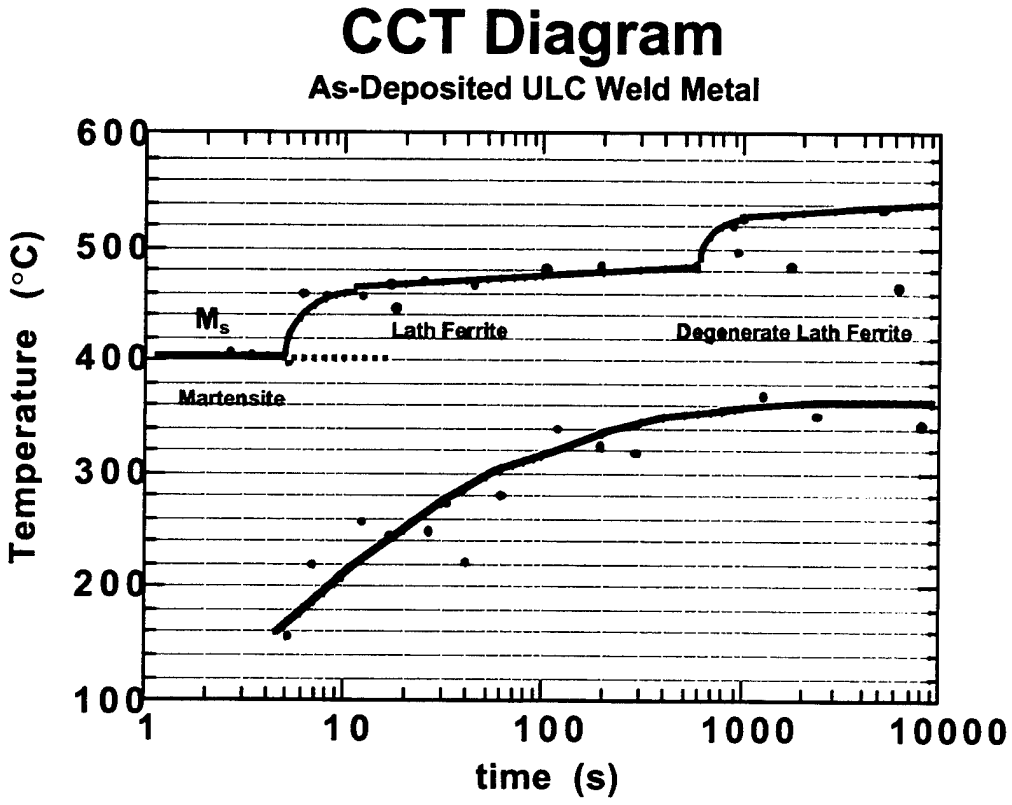

Figure 11. CCT-diagram for CTC-08 as-deposited weld metal.

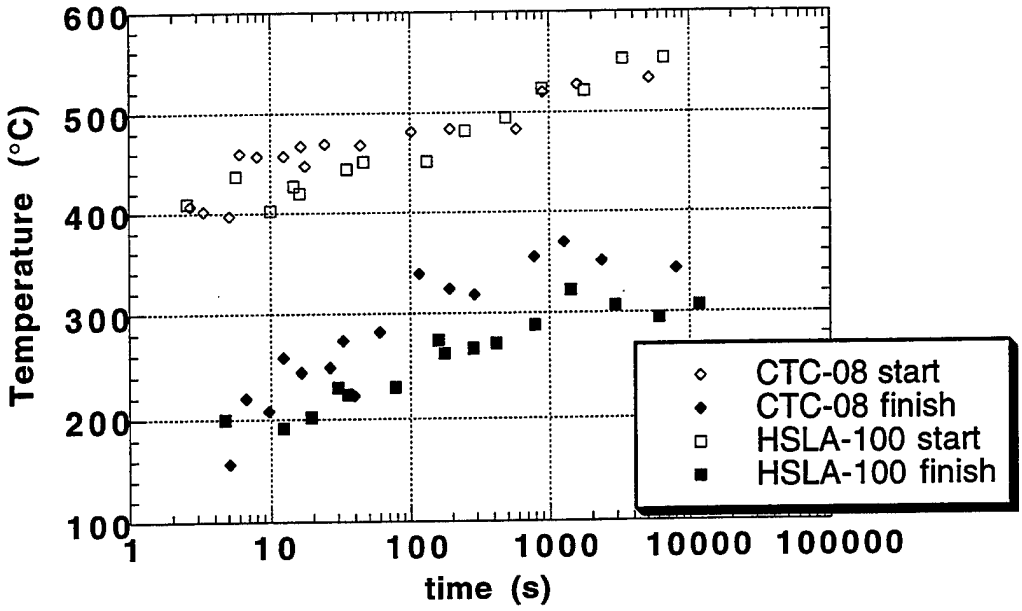

Figure 12. Comparison between CCT diagrams for CTC-08A as-deposited weld metal and HSLA-100 base plate.

higher transformation start temperature is observed. TEM analysis did not reveal any microconstituent other than degenerate ferrite (with some retained austenite and embedded inclusions) in these samples.

Comparison of the CCT diagram for the as-deposited weld metal to that of the HSLA-100 base plate (both for the same austenitizing treatment - 1200 °C for 15 minutes) shows a strong similarity between the two diagrams - see Fig. 12. The transformation finish temperatures are slightly higher for the as-deposited weld metal than for the HSLA base plate, but the form of the transformation curves (Figure 1) shows this to be a small difference, with less than about 5% of the base plate remaining untransformed at the time the weld metal has completed its transformation. The transformation start temperatures are nearly identical, with the only significant difference being that the ferrite curve of the as-deposited weld metal is shifted towards shorter reaction times. This similarity in transformation start temperatures is surprising, considering the large differences in chemical composition of the as-deposited weld metal (0.04% C) and the HSLA-100 base plate (0.07% C). The shift of the ferrite curve towards shorter reaction times is not unexpected, as oxide inclusions (which are present throughout the as-deposited weldment) have been shown to serve as nucleation sites for ferrite [8], and thus could enhance the kinetics of ferrite formation (although the inclusions observed here were relatively coarse and widely spaced).

Summary

There are thus at least five different microstructural regimes associated with this CCT diagram. These are listed below in order of increasing $t_{8/5}$ times (decreasing cooling rate),

corresponding to moving from transformation start (and finish) points on the left of Fig. 11 towards points on the right:

(1) $t_{8/5}$ = 1.1 s to 2.2 s; fully martensite - fine lath and coarse martensite, martensitic microhardness

(2) $t_{8/5}$ = 2.7 s to 8.5 s; predominantly martensite - long laths of ferrite with martensite and possibly ferrite between them, high microhardness typical of martensite. Not readily characterized by optical microscopy.

(3) $t_{8/5}$ = 14 s to 52 s; predominantly ferrite - packets of fine lath ferrite formed around the long laths, interstices filled in with martensite and ferrite, intermediate microhardness. Appears to be mostly to fully ferritic when viewed by optical microscopy, but actually has much higher martensite concentration.

(4) $t_{8/5}$ = 100 s to 301 s; fully ferrite - lath ferrite and degenerate ferrite.

(5) $t_{8/5}$ > 301 s; fully degenerate ferrite.

The application of optical microscopy to characterize these microstructures is particularly misleading at the intermediate cooling rates, when a combination of ferrite and martensite are formed. Due to the larger lath size of the ferrite and the limited resolution of optical microscopy, the amount of ferrite in these samples is severely overestimated. This research demonstrates that samples which appear mostly ferritic by optical microscopy may actually be predominantly martensitic, and that significant amounts of martensite may be present even when the samples appear fully ferritic by optical microscopy.

Work is in progress to correlate these microstructures with those observed in various regions of weldments prepared with this same CTC-08 consumable (i.e. in specimens from as-deposited weld metal that was not subsequently thermally treated in the dilatometer).

II. DILATOMETRIC AND MICROSTRUCTURAL ANALYSIS OF NCEMT CONSUMABLES, CTC03-R and CTC03-L

In collaboration with Paul Konkol of Concurrent Technologies Corporation (which operates NCEMT), two compositional variants of the top priority NCEMT ULC consumable, designated alloys CTC03-R and CTC03-L, were selected for dilatometric and microstructural analysis. These alloy designations refer to rich and lean alloy variations (particularly in terms of carbon concentration), respectively. Again, the compositions of these low carbon, Mn-Ni-Mo-Ti consumables are proprietary, but the carbon levels (0.035% for CTC03-R and 0.009% for CTC03-L) will be referred to throughout this report. As mentioned above, there was a concern about the compositional accuracy associated with a production heat. Standard errors for this type of fabrication were determined to be approximately ± 0.01 %C, ± 0.10 %Si, ± 0.20 %Ni, ± 0.15 %Mn, ± 0.05 %Mo, and ± 0.01 %Ti. [9,10]. For the low alloy content of these ULC alloys, such errors (particularly in carbon) can produce significant deviations from the intended composition. The goal of this project was to determine the effect of these potential variations on the transformation behavior and microstructure. The two alloys, CTC03-R and CTC03-L, were selected to represent the potential rich and lean compositional variants of such a process.

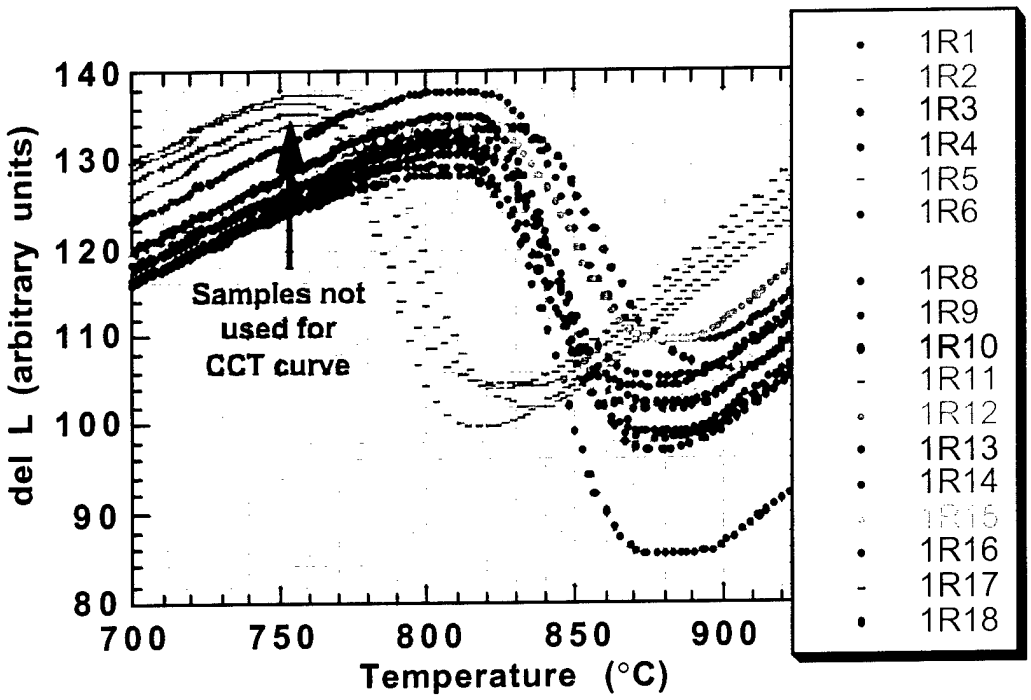

Fig. 13: Dilatometry curves during heating of CTC03-R specimens.

Experimental Procedure

The materials used in this study were obtained from ESAB (a weld consumable manufacturer) in the form of 4.7 mm diameter rods (i.e., before drawing down to final weld wire diameter) in order to facilitate machining of the 3 mm diameter dilatometry specimens. These rods were encapsulated in quartz under 1/3 atm argon and homogenized for 3 days at 1200 °C to remove any chemical inhomogeneities. Samples machined from these rods were then heated in a heating/quenching dilatometer to 950 °C where they were held for 15 minutes, and then cooled at various rates (from $t_{8/5}$ = 1 s to $t_{8/5}$ = 4000 s) with natural cooling, such that the cooling rate is proportional to the temperature difference between the sample and its surroundings. Unlabeled CCT diagrams were completed for the two CTC03 consumables, and microstructural and microhardness analyses were performed in order to fully document the transformation products and to label the CCT diagrams for both CTC03-L and CTC03-R. Since the CCT diagrams and TEM microstructures for the HSLA-100 base plate were already discussed in detail in previous reports and publications, they will only be mentioned here when comparisons are made to the CTC03-L and CTC03-R weld consumables.

Optical microscopy of the dilatometry samples was performed after standard metallographic polishing and etching with Nital. TEM analysis was performed on thin disks (0.5mm) cut from these dilatometry specimens, mechanically thinned to 50 μm, dimpled, and subsequently electropolished into thin foils.

Results and Discussion

Transformation Curves and "Unlabeled " CCT diagram

Thirty-eight samples (18 for CTC03-R and 20 for CTC03-L) were thermally cycled in the dilatometer with various cooling rates to develop the CCT diagrams. During heating, most of these samples transformed to austenite at about 800 °C. However, a significant minority of samples (4 for CTC03-R and 5 for CTC03-L) showed an anomalous behavior during heating - the beginning of the reaustenitization transformation for these samples was about 50°C lower than that of the other samples - Fig. 13. It is interesting to note that there was not a continuous variation in the reaustenitizing temperatures, but rather two discrete groupings of the specimens. Chemical analysis from a number of specimens has indicated that this behavior is not due to composition variations. In addition, the homogenization at 1200 °C for 3 days should have removed any effect of prior deformation (some regions of the as-received weld rod contained sharp bends which were straightened before machining of the samples). A definitive explanation for the different reaustenitizing temperatures in these specimens is thus not available at this time. Since these samples also often exhibited anomalous (lower) transformation start and finish temperatures during cooling, these specimens were not used in the construction of the CCT diagrams for either CTC03-R or CTC03-L.

From the transformation plots (Fig. 14) two important pieces of information can be determined: (1) the transformation start and finish temperatures, and (2) for the CTC03-R alloy, the volume fraction of austenite decomposed above the martensite start temperature, M_S.* This volume fraction can be considered to be a measure of the minimum amount of ferrite formed, since no martensite can form above the M_S, and microstructural observations (see below) have shown that no bainite forms in these alloys. For the CTC03-L alloy, it was not possible to unequivocally determine the M_S temperature, and thus the volume fraction of austenite decomposed above M_S, due to the very rapid ferrite transformation kinetics. The ferrite transformation in this alloy could not be completely suppressed even at the fastest cooling rate, obscuring the beginning of the martensite transformation. For both alloys, inflection points were observed in the transformation curves at the slowest cooling rates, indicative of a discrete change in the transformation behavior; e.g., see inflections at about 450 °C to 465 °C in the curves for $t_{8/5}$'s of 1998 and 3993 seconds in Fig. 14(a). Although such inflection points can be associated with the start of another transformation, no unique transformation product associated with these inflections was apparent from the TEM observations. The time-temperature coordinates of the inflection points were plotted on the CCT diagrams (see below) to delineate the discrete change in transformation behavior at those cooling rates.

The "unlabeled" versions of these CCT diagrams were constructed from the transformation curves and are presented in Figs. 15(a) and (b) along with the microhardness measurements. Although the general shapes of the transformation curves of the CTC03-L and the CTC03-R consumables are somewhat similar, the transformation start (and finish) curves are shifted to much higher temperatures and shorter times for CTC03-L, as expected, since it has a much lower carbon concentration (0.009%) than CTC03-R (0.035%). The CCT curve for the

*The M_S was determined by the dilatometry experiments to be about 425 °C for this alloy.

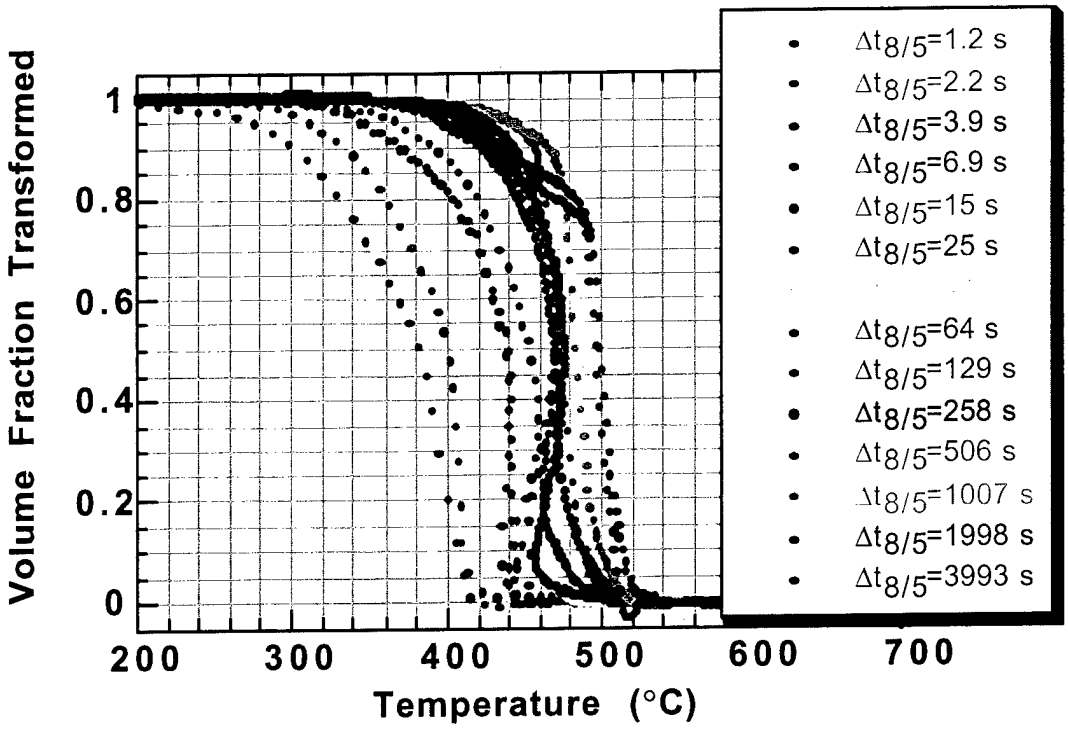

Figure 14(a). Transformation curves for CTC03-R consumable.

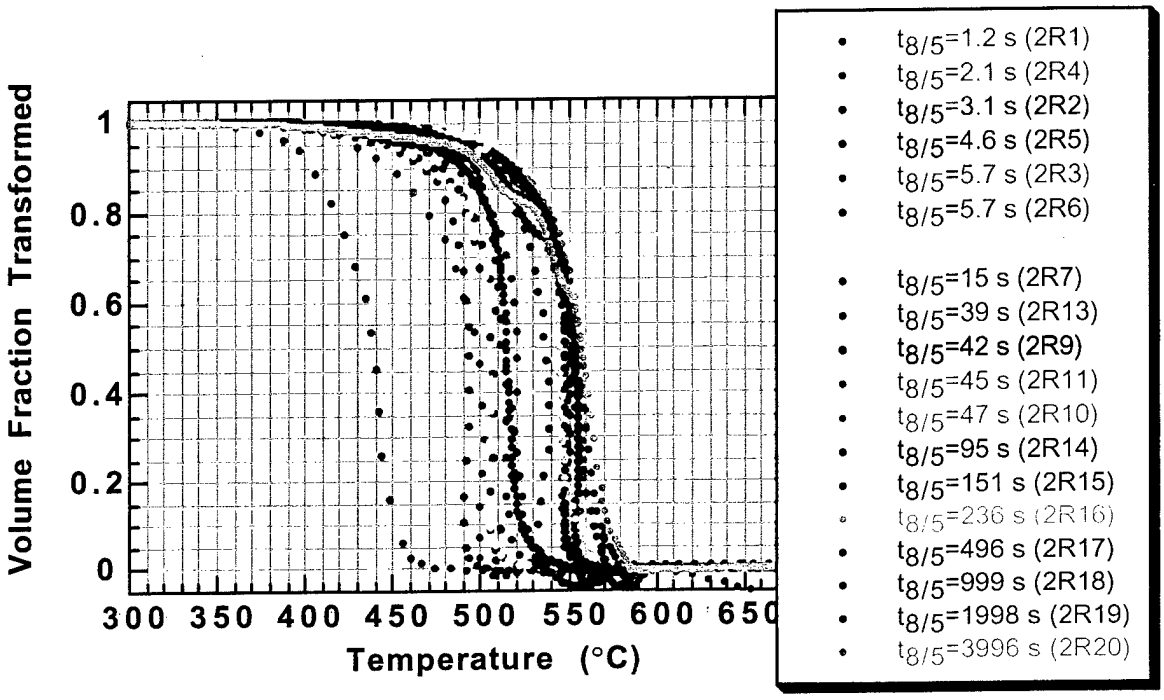

Figure 14(b). Transformation curves for CTC03-L consumable.

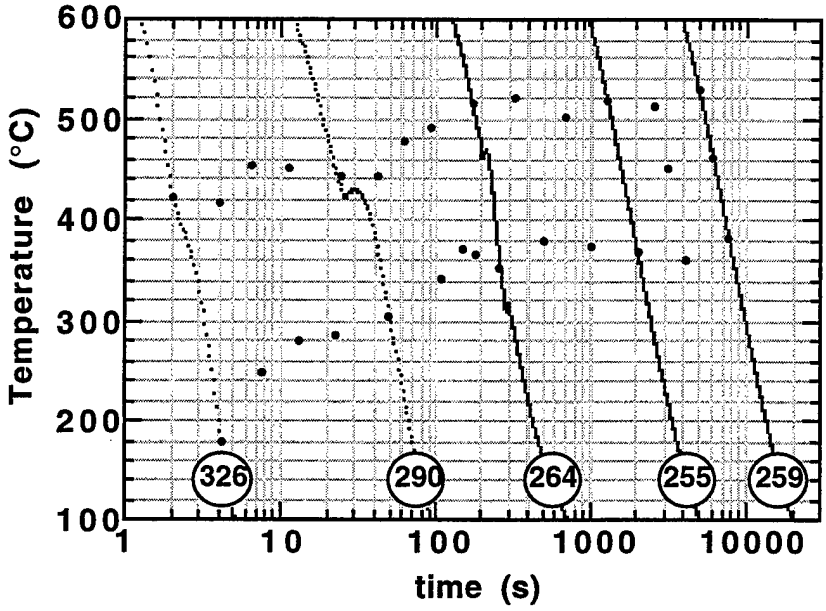

Figure 15(a). Unlabeled CCT-diagram with superimposed microhardness values (H_v) for CTC03-R consumable.

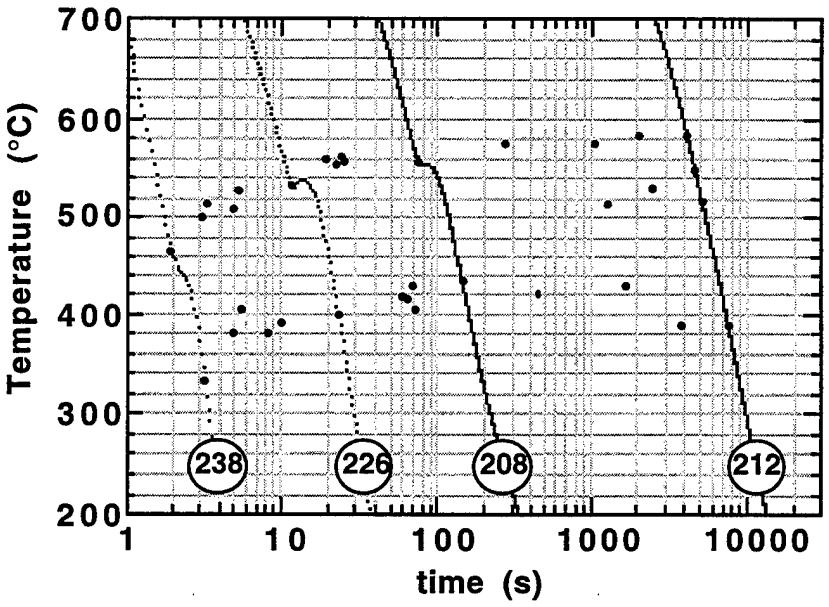

Figure 15(b). Unlabeled CCT-diagram with superimposed microhardness values (H_v) for CTC03-L consumable.

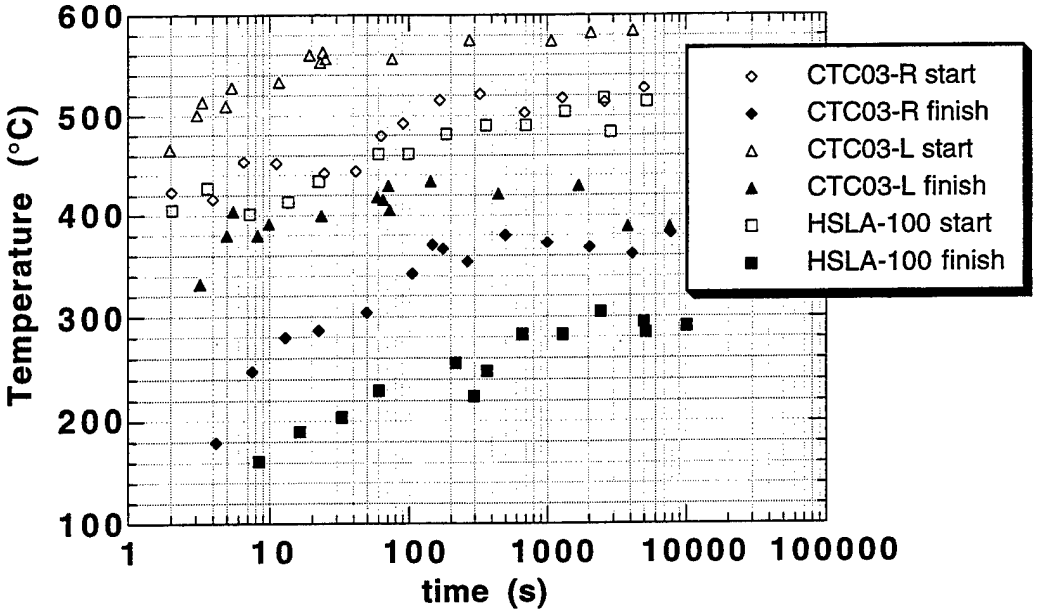

Figure 16. Comparison between CCT diagrams for the CTC03-R and CTC03-L consumables and the HSLA-100 base plate.

CTC03-R alloy is very similar to the CCT curves of both the HSLA-100 base plate and the as-deposited CTC-08 weld metal - see Figs. 12 and 16. Again, this is surprising considering the compositional differences (particularly carbon) between this consumable and the base plate. On the other hand, transformation of the CTC03-L alloy would be nearly complete before the HSLA-100 starts to transform (Fig. 16). This large difference in transformation temperatures between the CTC03-L consumable and the HSLA-100 base plate could be potentially detrimental. Diffusable hydrogen would tend to diffuse from the already transformed weld metal to the mostly untransformed base plate during cooling due to both the much lower solubility and the much higher diffusion rate of hydrogen in ferrite (or martensite), relative to austenite [11]. The resultant accumulation of hydrogen in the heat affected zone (HAZ) of the base plate would enhance the local susceptibility to hydrogen-assisted cracking. We had previously determined that large quantities of hard untempered martensite, which is susceptible to hydrogen-assisted cracking, form in the HAZ of welds made with the HSLA-100 base metal irrespective of heat input (i.e., cooling rate) [12], suggesting that hydrogen-assisted cracking is a particular concern for these welds. Subsequently, hydrogen-assisted cracking in the HAZ's of HSLA-100 weldments has been confirmed by work at NSWC [13] and Newport News Shipbuilding [14].

Microhardness

The microhardness of samples thermally cycled at various cooling rates typical of the different regimes of the CCT curves was measured to support the microstructural analysis. It is obvious from these measured microhardnesses (Figures 15(a) and 15(b)) that the microhardness of the rich alloy is much (50 to 90 H_V) higher and displays more variation with cooling rate than that of the lean alloy. These differences point to large variations both in the transformation

behavior and in the mechanical properties between these two alloys. This is consistent with macroscopic mechanical properties tests (particularly yield strength and transverse tensile strength) performed for NCEMT [15].

Both alloys show a general trend of lowered microhardness with decreasing cooling rates at fast to intermediate cooling rates; the microhardness remains essentially constant (within experimental error) for the slower cooling rates. This trend of decreasing microhardness with increasing cooling times can be generally explained by the formation of more ferrite during the slower cooling cycles (i.e. the higher $t_{8/5}$'s), as would be expected. This trend is in agreement with the CCT diagrams, which showed a general trend towards increasing start temperature (indicative of either ferrite or bainite, as opposed to martensite) with slower cooling rate. Microstructural analysis must be performed in order to determine what specific microconstituents or combination of microconstituents are responsible for these microhardness trends - e.g., polygonal ferrite, lath ferrite, degenerate ferrite, upper bainite, lower bainite, lath martensite, and/or coarse autotempered martensite.

Microstructural Analysis

Transmission Electron Microscopy (TEM) and optical microscopy were performed on the dilatometry specimens in order to understand the microstructural evolution in these materials and to label the phase fields on the CCT diagrams. Microstructural analysis was performed on 9 dilatometry specimens chosen to represent the various microstructural regimes of the two CCT curves (cooling curves of these specimens are shown in Figure 15). Optical microscopy results from these samples are shown in Figures 17 and 18. Through a wide range of intermediate and slow cooling rates, the rich alloy (Figure 17) forms a similar microstructure of coarse ferrite laths. Through the entire range of cooling rates, the lean alloy (Figure 18), however, produces a coarse microstructure characteristic of what has been termed (at this level of resolution) ferrite with non-aligned second phase (FS(NA)).

TEM analysis is required because the microstructures in these ultra low carbon steels are too fine to be adequately resolved by optical microscopy alone, leading to an overestimation of the coarser (usually ferritic) phase, as demonstrated in the above study of the as-deposited weld metal. In order to provide for a representative sampling of the microstructure, hundreds of TEM micrographs were taken from the 9 selected dilatometry specimens. Representative TEM micrographs of fine lath and coarse plate martensite, elongated lath ferrite, and degenerate lath ferrite are shown in Fig. 19. All of the microscopy and microhardness observations were then correlated to label the CCT diagrams for the CTC03-L and CTC03-R weld consumables (all for a 950 °C austenitizing temperature).

The reaction products for the CTC03-R alloy are fine lath martensite mixed with some coarse martensite at the fastest cooling rates, a mixture of lath martensite and lath ferrite at fast cooling rates, and a coarse lath ferrite at intermediate to slow cooling rates which becomes more degenerate with decreasing cooling rate. These are similar to the microstructures observed in the CTC-08 as-deposited weld metal with the primary difference being the large scale of the ferrite laths observed in CTC03-R. On the other hand, the CTC03-L alloy only contained a small amount of lath martensite even at the fastest cooling rate, and no martensite was observed for any other cooling rate. In addition, the ferrite in this CTC03-L alloy rapidly evolves from the fine

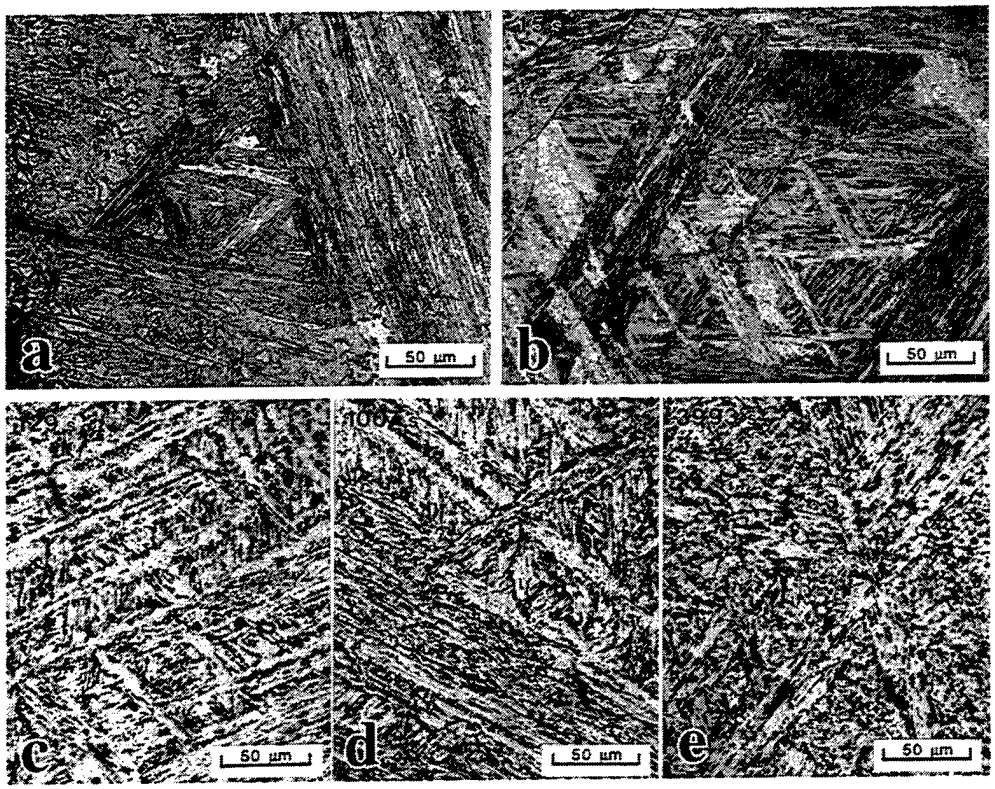

Figure 17. Optical micrographs of CTC03-R dilatometry specimens for cooling rates corresponding to $t_{8/5}$ times of (a) 1.2 s, (b) 15 s, (c) 129 s, (d) 1007 s, (e) 3993 s.

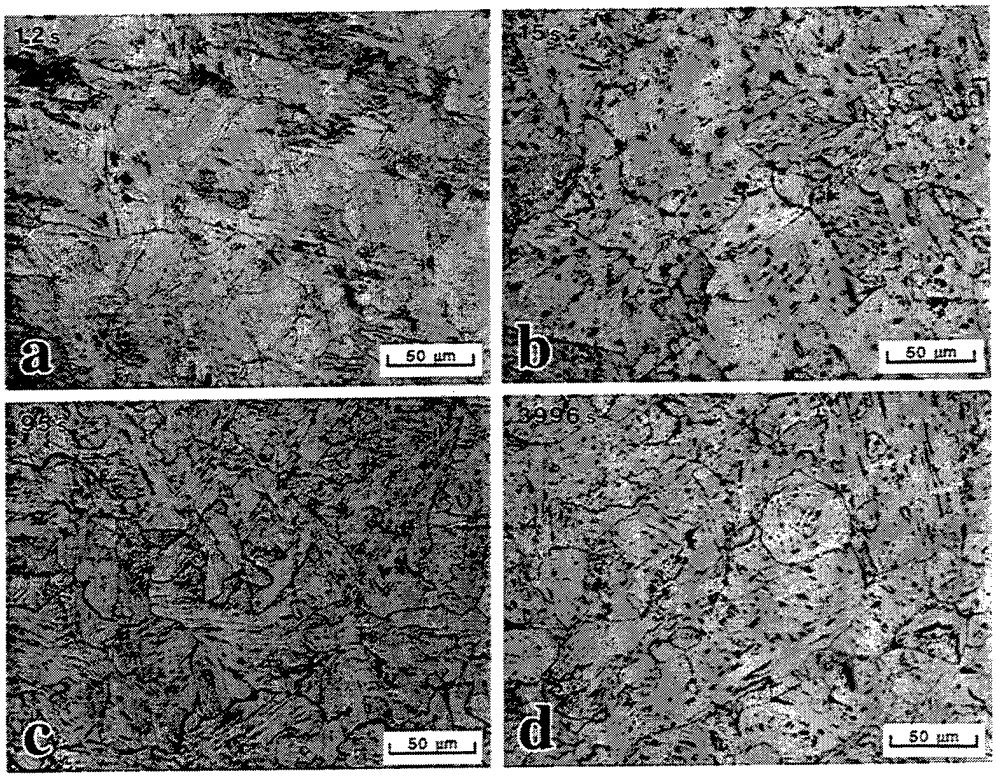

Figure 18. Optical micrographs of CTC03-L dilatometry specimens for cooling rates corresponding to $t_{8/5}$ times of (a) 1.2 s, (b) 15 s, (c) 95 s, (d) 3996 s.

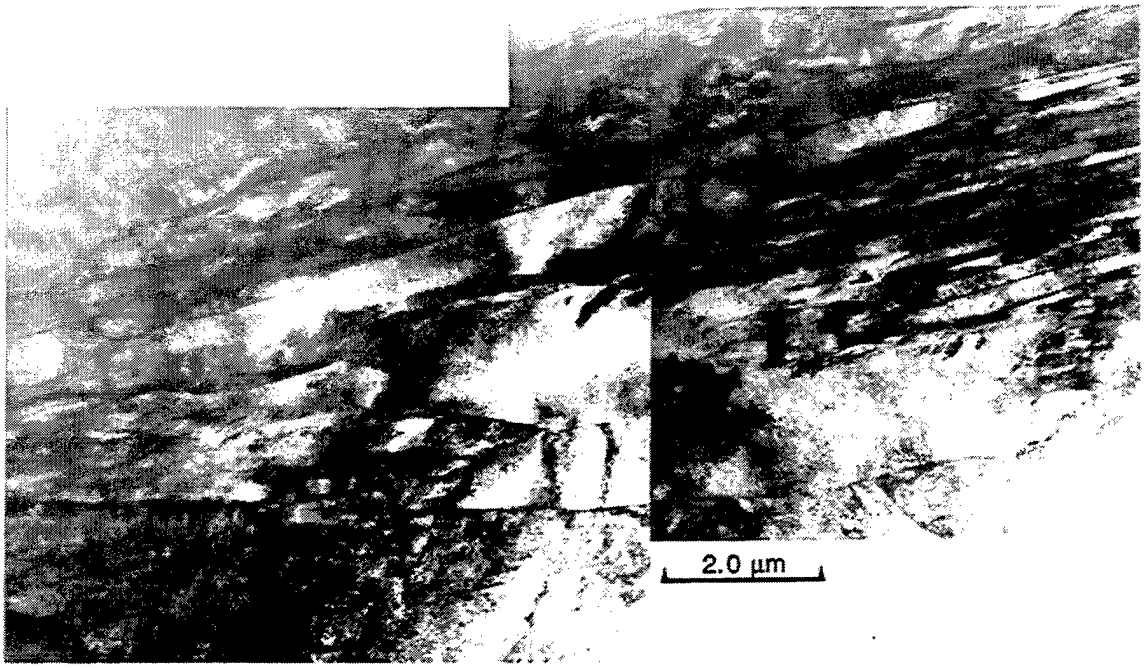

Figure 19(a). TEM montage of both coarse plate and fine lath martensite in CTC03-R specimen subjected to a fast cooling rate ($t_{8/5}$ time of 1 sec.).

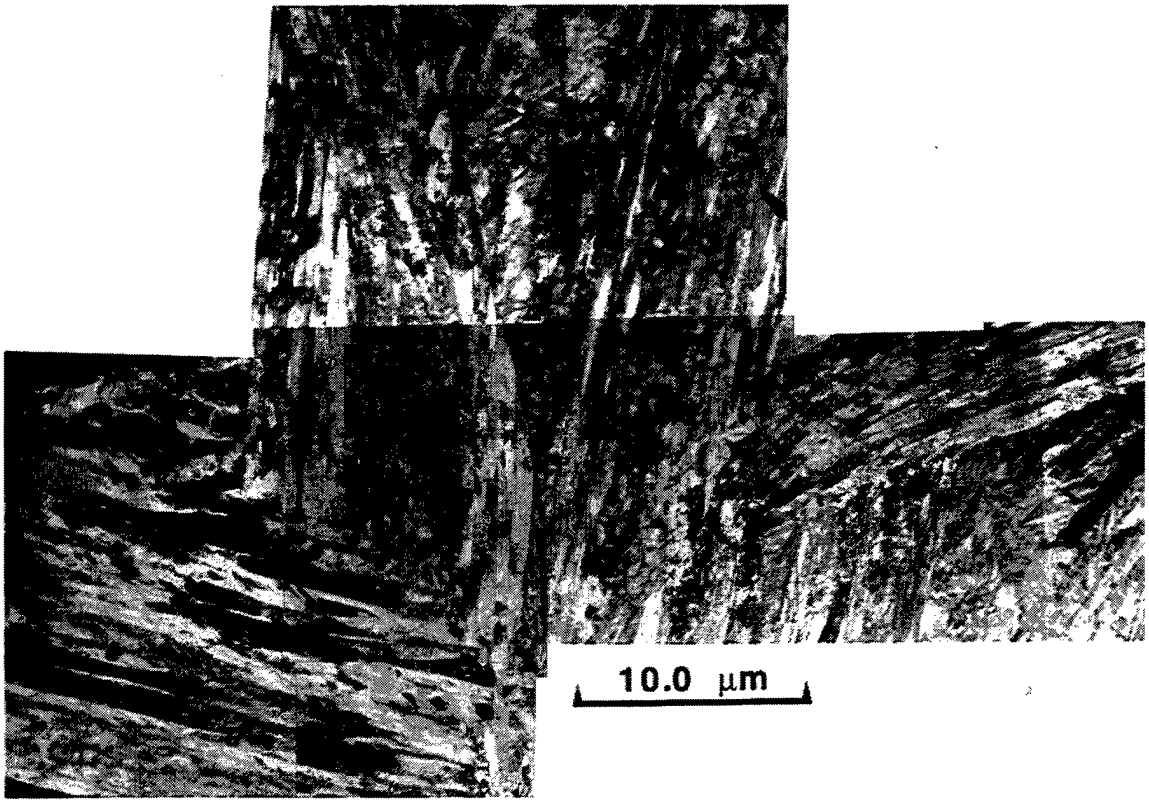

Figure 19(b). TEM montage of lath ferrite and lath martensite in CTC03-R specimen subjected to a cooling rate with $t_{8/5}$ = 16 sec.

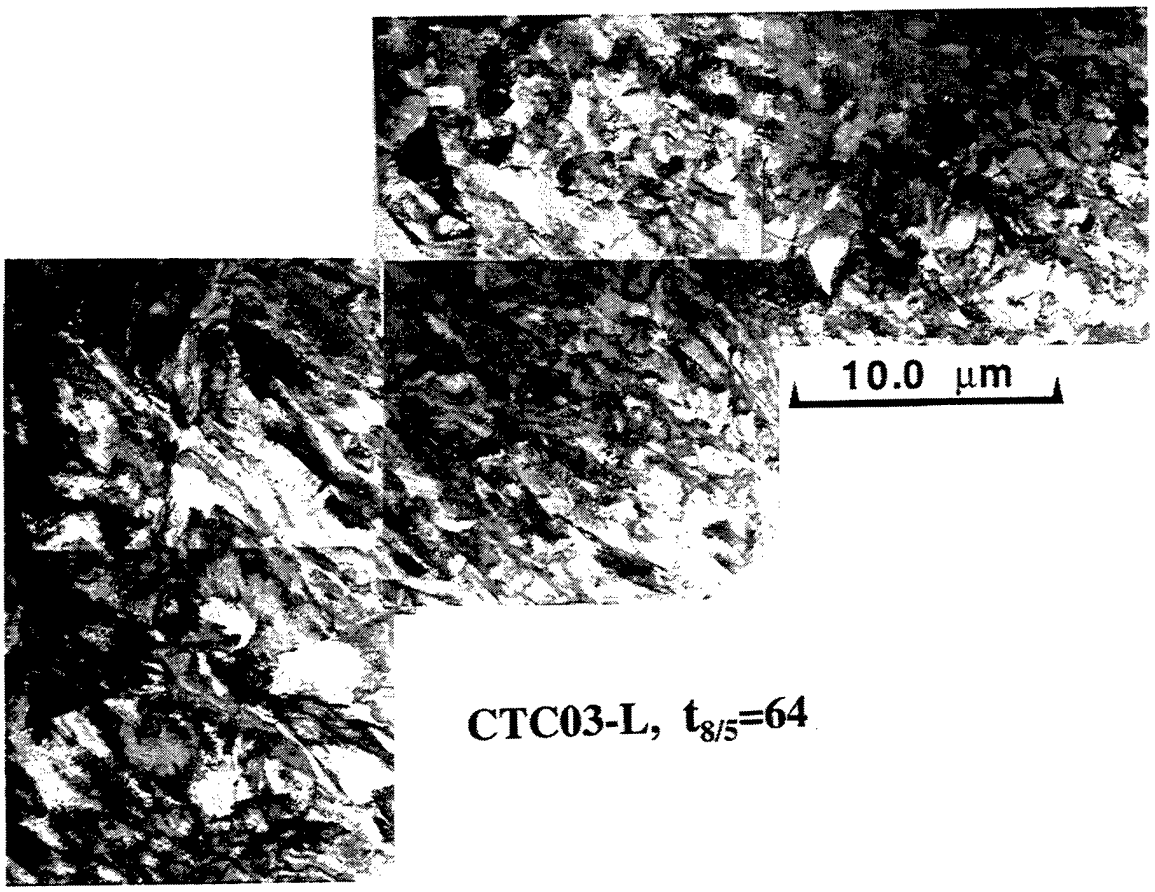

Figure 19(c). TEM montage of degenerate ferrite in CTC03-R specimen subjected to a cooling rate with $t_{8/5}$ = 64 sec.

lath ferrite observed at the fastest cooling rate to a coarser lath ferrite which becomes highly degenerate at much faster cooling rates than either the CTC03-R alloy or the as-deposited CTC-08 weld metal. Thus, the rich alloy consumable (CTC03-R) is much more martensitic at the faster cooling rates (and is even more martensitic than the as-deposited weld metal), as would be expected from the higher carbon equivalent of that alloy while the lean alloy consumable (CTC03-L) has a much higher concentration of the soft degenerate ferrite throughout a wide range of moderate to slower cooling rates.

For both CTC03 alloys (as well as for the as-deposited CTC-08 weld metal), the morphology of the degenerate ferrite becomes increasingly "blocky" or "equiaxed" as the cooling rate is decreased, and interlath ferrite:ferrite boundaries are often difficult to discern, but can usually be revealed with appropriate tilting of the sample in the TEM. Although similar morphologies have sometimes been referred to in the literature as "polygonal ferrite", it is important to recognize that at least in these materials, what appear by optical microscopy (and at first glance in the TEM) to be large equiaxed ferrite crystals are often not monolithic as polygonal ferrite would be, but instead are composed of a number of ferrite crystals which have ferrite:ferrite boundaries between them - e.g., see Figs. 10 and 19(c). These ferrite: ferrite grain boundaries often appear very faint or invisible, and can only be revealed by repeated tilting experiments in the TEM. Also, the highest transformation start temperatures observed in any of

these alloys was 580°C for CTC03-L, 530°C for CTC03-R, and 540°C for the as-deposited CTC-08 weld metal, even at the slowest cooling rates. These temperatures are well below the transformation temperature typically reported in the literature for polygonal ferrite in lower carbon alloys (e.g., about 800°C for HSLA-100 [16] and 700 °C for a modified A710 steel [17]), for similar cooling rates to those used here. Thus, we maintain that the microstructures observed in these consumables at low cooling rates are not conventional polygonal ferrite, and have instead labeled these microstructures as "degenerate lath ferrite" due to their similarity to the lath ferrite present at faster cooling rates

Retained austenite was occasionally observed in very small amounts between ferrite and/or austenite laths in the CTC03-R alloy, but was never seen in the CTC03-L alloy. In contrast, much more retained austenite was observed in the HSLA-100 base plate material and the CTC-08 as-deposited weld metal. The coarse plate martensite often present in the HSLA-100 base plate and in the CTC-08 as-deposited weldments was not observed in CTC03-L, but was observed (in the untempered condition) in CTC03-R at the fastest cooling rate. Finally, neither carbides nor fine solid-state precipitates of any type were ever observed in either of these two CTC03 alloys, although a small number of spherical inclusions were occasionally imaged (e.g., see left side of Fig. 19(b)). As would be expected, many more inclusions were observed for the as-deposited CTC-08 weld metal discussed in the previous section (see Fig. 6).

CCT Diagrams with Labeled Phase Fields

Based on the microstructural and microhardness observations, the CCT diagrams for the CTC03-R and CTC03-L weld consumables can now be labeled, as shown in Figs. 20(a) and 20(b), respectively. Rather than discuss individually the microstructure corresponding to each cooling rate (as was done for the CTC-08 *as-deposited* weld metal), the microstructural evolution will be briefly summarized for the CTC03-R and CTC03-L consumables. The CTC03-R alloy (Figure 20(a)) exhibits similar overall trends in transformation behavior to the CTC-08 as-deposited weld metal and the HSLA-100 base plate, with fine lath martensite mixed with the coarse martensite at the fastest cooling rates (to the left of the CCT diagrams), a mixture of lath martensite and lath ferrite at fast cooling rates, and lath ferrite at intermediate to slow cooling rates which becomes more degenerate with decreasing cooling rate. However, the small difference between the lath ferrite transformation temperature and the martensite start temperature in CTC03-R, as compared to the CTC-08 as-deposited weld metal or HSLA-100 base plate, indicates that this alloy may not produce enough ferrite at the moderately fast cooling rates to ensure the proper combination of strength and toughness sought after in these alloys. Indeed, mechanical tests performed for NCEMT reveal that at faster cooling rates, the yield strength of the CTC03-R alloy became too high at cooling rates greater than about 28 °C/s [15], which is midway across the lath ferrite phase field. Significant recalescence at cooling rates slower than this allow additional reaction time for the formation of ferrite, decreasing the yield strength to acceptable levels.

The CTC03-L alloy (Figure 20(b)), on the other hand, produces only a minor amount of martensite at the fastest cooling rate and is fully ferritic throughout the intermediate and slow cooling rates. Only the fine lath martensite was observed in this alloy; no coarse martensite was observed in CTC03-L, presumably due to the low carbon concentration of this alloy. The ferrite, which has a fine lath morphology at the fastest cooling rate, rapidly evolves into a coarse lath

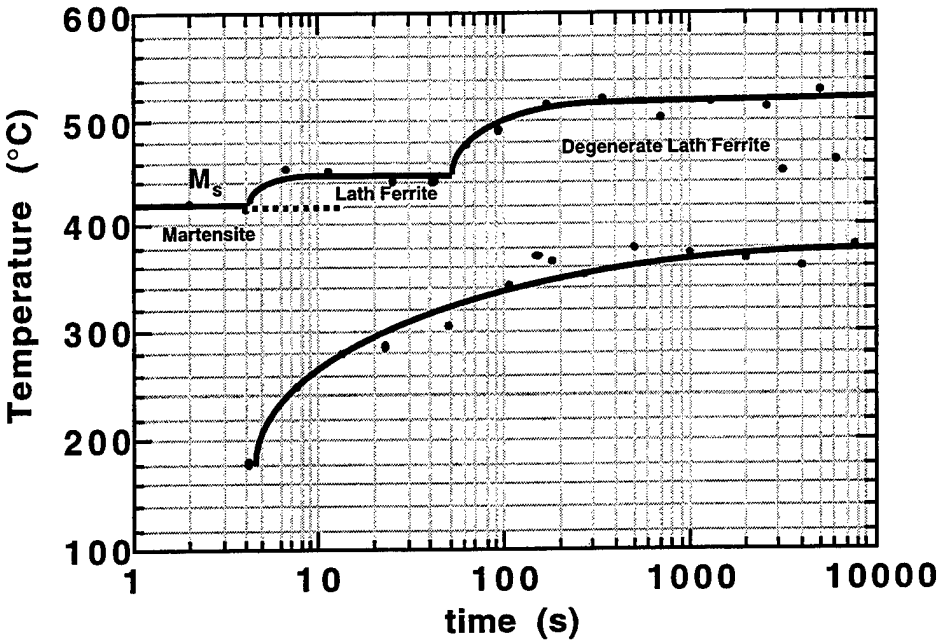

Figure 20(a): CCT Diagram of CTC03-R consumable.

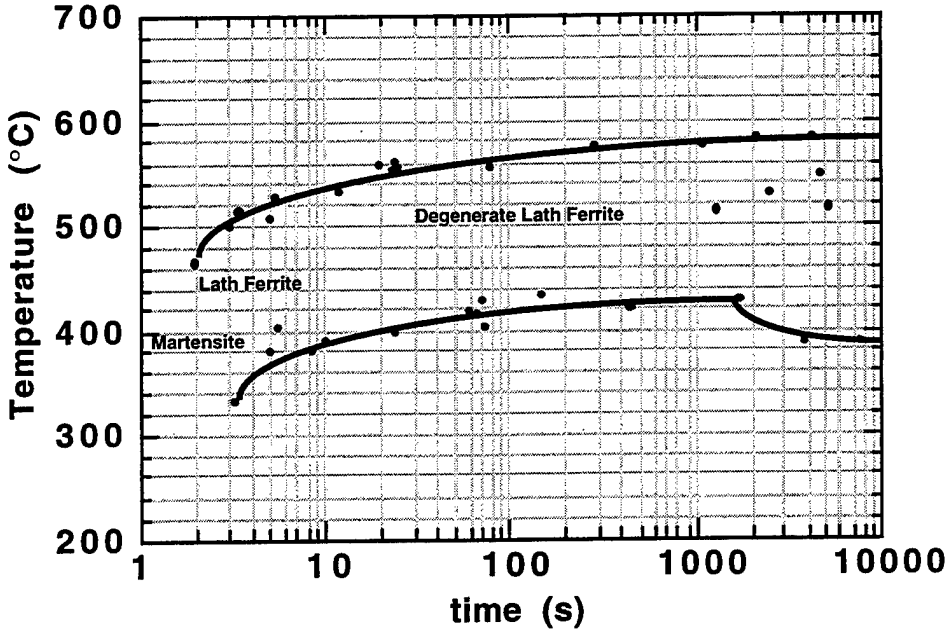

Figure 20(b): CCT Diagram of CTC03-L consumable.

ferrite which becomes degenerate at intermediate to slow cooling rates. This preponderance of degenerate ferrite throughout much of the range of cooling rates suggests that these alloys will tend to have insufficient strength. Again, this prediction was borne out in the mechanical tests conducted for NCEMT [15], which showed that the transverse weld tensile strength was insufficient for cooling rates less than about 28 °C/s, i.e., only the fastest 5 cooling rates would satisfy these strength requirements.

Thus, there is in general a higher proportion of martensite for the CTC03-R alloy (as compared to CTC03-L), as expected due its higher carbon concentration, while ferrite was more prevalent (and more degenerate) for the CTC03-L alloy. In addition, both coarse martensite and small amounts of interlath retained austenite were observed in CTC03-R, but neither were ever observed for CTC03-L at any cooling rate. The amounts of retained austenite observed in CTC03-R were less than observed in either the as-deposited CTC-08 weld metal or the HSLA-100 base plate.

SUMMARY AND CONCLUSIONS

Comparison between the rich and lean variants of the CTC03 weld consumable demonstrate that compositional variations expected from typical production heats will produce significant variations in the transformation behaviors, the final microstructures, and the final properties of weldments made from those consumables. The transformation temperatures of the lean alloy are 60 °C to 100 °C higher than those of both the rich alloy and the HSLA-100 base plate, which could potentially lead to enhanced hydrogen-assisted cracking in the base plate due to hydrogen ingress from the fusion zone of the lean alloy into the base plate HAZ. There are large variations in both the microstructures and the transformation behaviors of the rich and lean alloys, suggesting a large disparity in the mechanical properties throughout the range of potential cooling rates. These predicted large variations in mechanical properties are demonstrated by the observed variations in microhardness, with the lean alloy from 50 to 90 H_v softer than the rich alloy, and are further confirmed by other mechanical tests (tensile and Charpy impact) conducted for NCEMT. This research demonstrates that the compositional variations expected from production heats can cause extensive variations in the transformation behavior, microstructure, and microhardness of these ULC consumables. Since current fabrication practices would generate similar compositional variations for any comparable ULC alloy, additional steps need to be taken to ensure the chemical homogeneity, and thus uniform weld properties, of the ULC weld consumables.

The CCT diagrams and detailed microstructural analyses developed in this research program for the HSLA-100 base plate, the CTC-08 as-deposited weld metal, and the CTC03-R and CTC03-L NCEMT consumables should all provide a baseline for understanding microstructural evolution during welding of HSLA plate steels with ultra low carbon consumables, which has direct relevance to Naval applications. As mentioned earlier, these CCT diagrams should be valuable for scientists, engineers and designers in the development, processing and use of such new alloys for welding applications.

ACKNOWLEDGMENTS

We are grateful for the financial support provided for this work from the Industrial Programs Office of the Office of Naval Research (Code 36) under grant reference number N0001497AF00002. Appreciation is expressed to Paul Konkol and Bruce Somers at NCEMT for many helpful discussions, and to Paul Konkol and Susan Fiore (of ESAB) for providing the weldments and weld rods used in this investigation. Appreciation is expressed to Ed Pierpoint for performing the dilatometry and to Michael Mangan for performing some of the Transmission Electron Microscopy.

REFERENCES

1. G. Tither, "The Development and Applications of Niobium-Containing HSLA Steels", HSLA Steels: Processing, Properties and Applications, TMS, Warrendale, PA (1992) pp. 61-80.
2. J. J. Deloach, Jr., "An Overview of the US Navy Filler Metal Development Program", Welding and Weld Automation in Shipbuilding, ed. R. Dinale, TMS, Warrendale PA (1996) pp. 85-104.
3. E. J. Czyryca, R. E. Link, R. J. Wong, D. A. Aylor, T. W. Montemarano, and J. P. Gudas, "Development and Certification of HSLA-100 Steel for Naval Ship Construction," *Naval Engineers Journal* **102**(3), 63-81 (1990).
4. P. L. Harrison and R. A. Farrar, "Application of Continuous Cooling Transformation Diagrams for Welding of Steels," *Int. Mater. Rev.* **34**(1), 35-51 (1989).
5. R. A. Farrar, Z. Zhang, S. R. Bannister, and G. S. Barritte, "The Effect of Prior Austenite Grain Size on the Transformation Behavior of C-Mn-Ni Weld Metal," *J. Mat. Sci.* **28**, 1385-1390 (1993).
6. "Guide to the Light Microscope Examination of Ferritic Steel Weld Metals," IIW Doc. No. IX-1533-88/IXJ-123-87 Revision 2, June 1988.
7. R. W. Fonda, G. Spanos, and R. A. Vandermeer, "Observations of Plate Martensite in a Low Carbon Steel," *Scripta Met. et Mat.* **31**(6), 683-688 (1994).
8. D. J. Abson, R. E. Dolby, and P. H. M. Hart, Proceedings of the Conference on Trends in Steels and Consumables for Welding, The Welding Institute, Abington (1979) pp. 75-101.
9. B. R. Somers, National Center for Excellence in Metalworking Technology, private communication.
10. P. J. Konkol and K. Sampath, "Commercialization of Advanced Welding Consumables for Welding HSLA-80 and HSLA-100 Steels, Rich and Lean Composition Variations of Advanced MIL-100S and MIL-120S Electrodes." TR No. 95-151, National Center for Excellence in Metalworking Technology, Johnstown, PA, Jan. 1996.
11. W. W. Wang, R. Wong, S. Liu, and D. L. Olson., "Use of Martensite Start Temperature for Hydrogen Control", Welding and Weld Automation in Shipbuilding, ed. R. Dinale, TMS, Warrendale PA (1996) pp.17-31.
12. R. W. Fonda, G. Spanos, and R. A. Vandermeer, "Processing-Microstructure-Property Relationships in HSLA-100 Steel Weldments," Proceedings of the 4th International Conference on Trends in Welding Research, ASM International, Metals Park, OH (1996) pp.277-282.
13. R. Wong, "Hydrogen Cracking Resistance of High Strength Steels in Single Pass and Multiple Pass Weldability Tests", Welding and Weld Automation in Shipbuilding, ed. R. Dinale, TMS, Warrendale PA (1996) pp.33-46.
14. J. Sawhill, Newport News Shipyard, private communication (1996).
15. B. R. Somers and P. J. Konkol, "Commercialization of Advanced Welding Consumables for HSLA-80 and HSLA-100 Steels; Evaluation of Rich and Lean Experimental MIL-100S

Compositions at Newport News Shipbuilding," TR No. 97-089, National Center for Excellence in Metalworking Technology, Johnstown, PA, Aug. 1997.

16. A. D. Wilson, E. G. Hamburg, D. J. Colvin, S. W. Thompson, and G. Krauss, "Properties and Microstructures of Copper Precipitation Aged Plate Steels," Proceedings of Microalloying '88, World Materials Congress, American Society for Metals, Metals Park, OH (1988) pp. 259-275.
17. S. W. Thompson, D. J. Colvin, and G. Krauss, "Continuous Cooling Transformations and Microstructures in a Low-Carbon, High-Strength Low-Alloy Plate Steel," *Met. Trans. A* **21A**, 1493-1507 (1990).